

# Neuron

## Supplemental Data

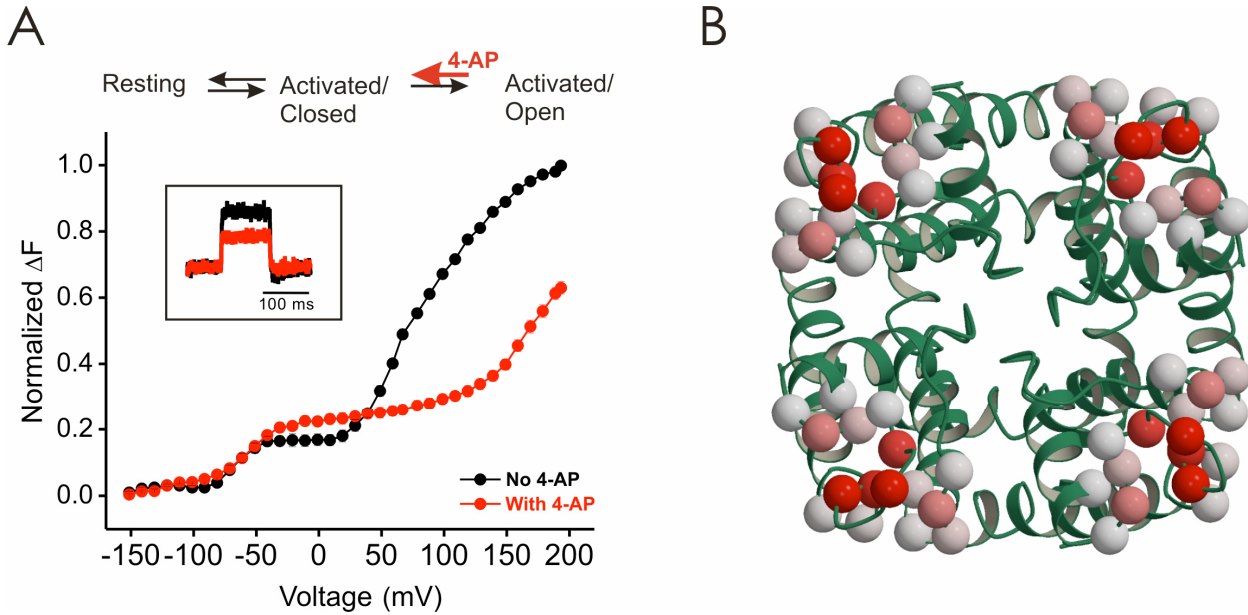
### Closing in on the resting state of the Shaker K<sup>+</sup> channel

Medha M. Pathak<sup>\*</sup>, Vladimir Yarov-Yarovoy<sup>\*</sup>, Gautam Agarwal, Benoît Roux, Patrick Barth, Susy Kohout, Francesco Tombola and Ehud Y. Isacoff

## Supplemental Results

### Fast ΔFs in the pore domain turret track channel opening

We analyzed the fluorescence report in detail at K427C, one of the PD sites in the turret that shows a large fast  $\Delta F$  signal. We recorded from K427C-TMRM channels in the background of two other kinds of mutations: a) the non-conducting mutation W434F, that locks channels in the P-type inactivated state, but does not prevent the normal voltage sensing steps or the channel opening steps from taking place (Loots and Isacoff, 1998; Perozo et al., 1993; Yang et al., 1997), and b) the ILT triple mutant, which stabilizes the activated-not-open state of the channel, thus separating the processes of voltage sensing and opening by a large voltage range (Ledwell and Aldrich, 1999; Pathak et al., 2005). The  $\Delta F$  of K427C-TMRM/ILT/W434F channels had two components, a minor component that took place over the voltage range shown earlier to correspond to voltage sensing in the ILT mutant channel, and a major component, which occurred over the voltage range shown earlier to correspond to opening in the ILT mutant channel (**Figure S1A**) (Ledwell and Aldrich, 1999; Pathak et al., 2005). This strongly suggests that the major  $\Delta F$  component for TMRM attached to site K427C corresponds to the opening step rather than to voltage sensing. To further test this, we employed an additional assay, which used 4-aminopyridine (4-AP) to alter selectively the final transition from activated/closed to activated/open, as shown earlier (Armstrong and Loboda, 2001; McCormack et al., 1994) (**Figure S1A, top**). 4-AP had little effect on the minor component of the  $\Delta F$  at the more negative voltage range, consistent with previous observations (Armstrong and Loboda, 2001; Pathak et al., 2005), but produced a big rightward shift (100mV) of the major component of the  $\Delta F$ , consistent with this being the opening step.



**Supplementary Figure S1. Fast  $\Delta F$  in pore domain tracks opening**

**(A)** State diagram showing a simplified pathway for channel opening from the resting state (top). In the presence of 4-AP the backward reaction from the Activated/open to the Activated/closed state (red arrow) is accelerated (Armstrong & Loboda, 2001). (bottom) F-V curves for K427C-TMRM ILT W434F in the absence (black curve) and in the presence (red curve) of 3 mM or 4 mM 4-AP in the bath solution. No difference in behavior was observed between the two concentrations; hence data from both are pooled. Data are mean from 12 cells; error bars show standard error of the mean and are smaller than the symbol for most points. Inset shows fluorescence traces in response to a voltage step to +190 mV in the absence (black) and presence (red) of 4-AP.

**(B)** Amplitude of fast  $\Delta F$ s color-coded according to the scale used in **Figure 3C**, (where pure white corresponds to no fast  $\Delta F$  and pure red corresponds to largest fast  $\Delta F$  seen in the channel) and painted onto the backbone atoms of pore domain of the Kv1.2 crystal structure.

**Figure S1B** shows the fast  $\Delta F$ s mapped on to the PD of the Kv1.2 crystal structure (Long et al., 2005a). Small or no fast  $\Delta F$ s are observed at the periphery of the PD, which would be close to the VSD. Several pore domain positions located away from the interface with the VSD had very large fast  $\Delta F$ s. These sites mapped to the turret and S6-P loop.

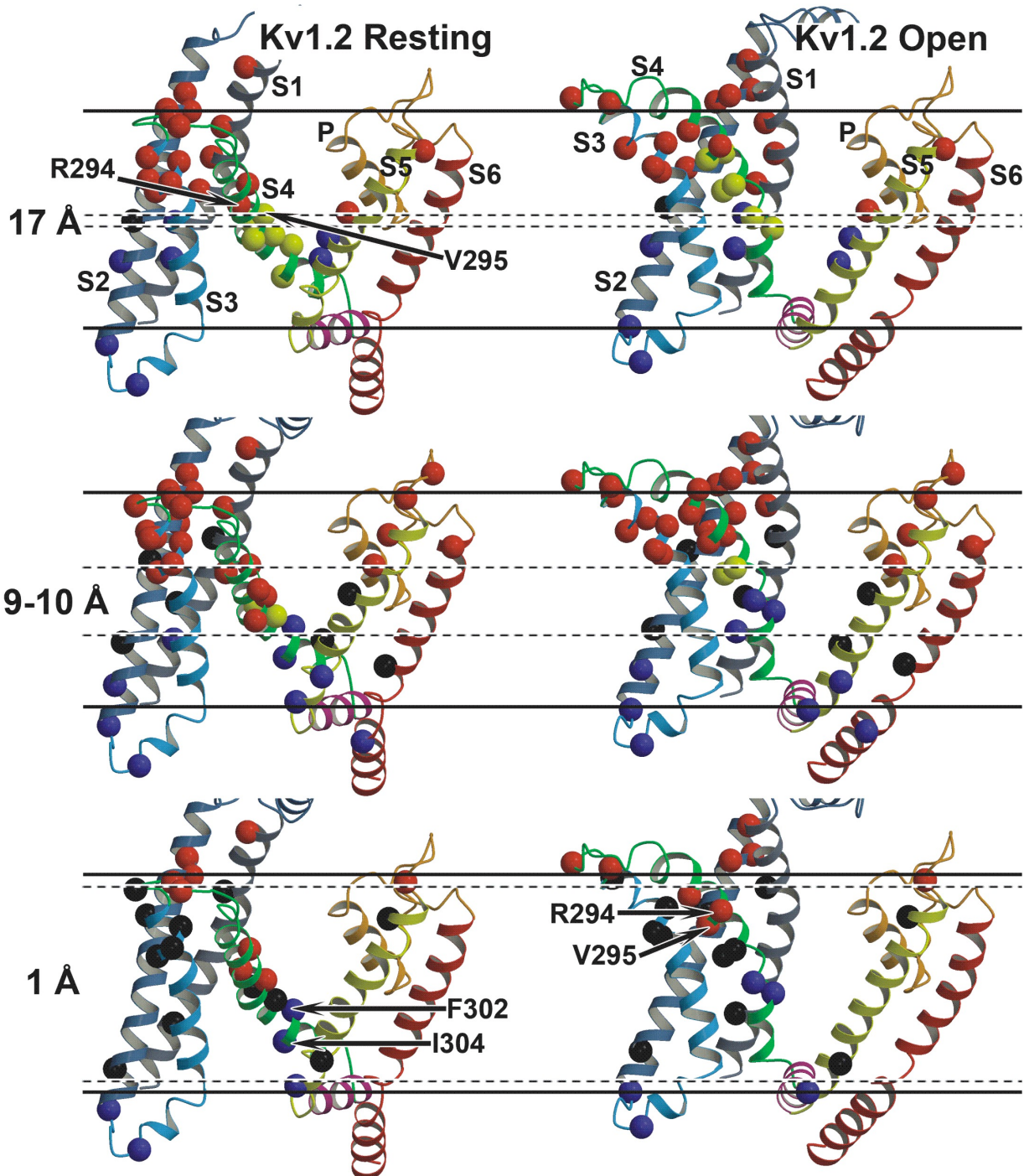
Taken together, these results indicate that the turret undergoes a conformational rearrangement during channel opening. This finding agrees with recent data from crystal structures of two closely related KirBac channels that capture the channel in different degrees of opening – the partially open KirBac 3.1 structure (1XL6) and the closed KirBac1.1 structure

(1P7B) (Gulbis JM, personal communication). Besides differences at the helix bundle crossing at the internal end of TM2, there are striking differences in the conformation of the turret, suggesting a coupled motion of the turret and the intracellular gate.

### Biotin-avidin data mapped onto the Kv1.2 resting and open state models

Our resting and open state models were compared with the biotin-avidin accessibility data obtained in KvAP (Ruta et al., 2005). The accessibility data for the KvAP PD were used to define the extracellular and intracellular boundaries of the 30 Å thick membrane. The relative position of S4 in our resting state model and the open state structure fit well with the data obtained with biotin attached to linkers that were 10 and 17 Å in length (see top and middle panels in **Figure S2 in the Supplemental Data**). For example, in our resting state model, the first S4 arginine (R1) (R294 in Kv1.2; R117 in KvAP; R362 in Shaker), which is inaccessible to intracellular avidin even with the 17 Å biotin linker (Ruta et al., 2005), is, in fact, ~17 Å from the intracellular side of the membrane (see upper left panel in **Figure S2 in the Supplemental Data**). Any further downward vertical movement of S4 would put R1 into <17 Å from the intracellular side of the membrane and disagree with the data.

The S4 position in our resting state model disagrees with the 1 Å biotin attachment data at two positions near its C-terminal end: F302 (F370 in Shaker) and I304 (I372 in Shaker) are 10 and 5 Å away, respectively, from the intracellular edge of the membrane in the model (see lower left panel in **Figure S2 in the Supplemental Data**). We suggest that the tilt angle of the intracellular end of S4 may differ between the Kv1.2 and KvAP channels in the resting state along with a difference in the tilt of the S4-S5 linker, which is positioned parallel to the plane of the membrane in our Kv1.2 resting state model, but maybe significantly tilted in the KvAP resting state, as was proposed by Long et al. (Long et al., 2005b) from the KcsA-based PD model. It should be noted that the S4 position in the Kv1.2 open state x-ray structure also disagrees with the 1 Å biotin attachment data at two positions near the N-terminal end of S4: R294 (R362 in Shaker) and V295 (V363) are 6 and 8 Å away, respectively, from the extracellular edge of the membrane (see lower left panel in **Figure S2 in the Supplemental Data**), suggesting either that the tilt of the extracellular end of S4 differs between Kv1.2 and KvAP in the open state, or that the S4 position in the Kv1.2 x-ray structure does not reflect its actual position in the open state.



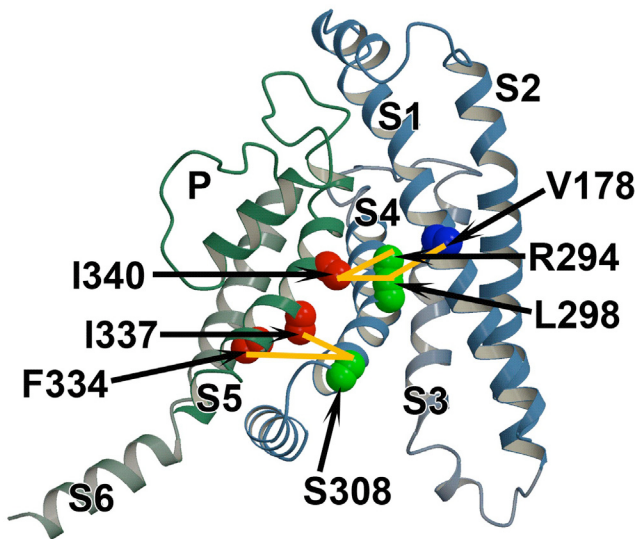
**Supplementary Figure S2. Biotin-avidin accessibility data for the KvAP channel residues mapped onto a single subunit of the Kv1.2 resting and open state models**

Transmembrane segment S1 colored grey and segments S2 through S6, and P-loop colored by rainbow scheme from blue to red and shown in ribbon representation. Solid bars indicate approximate location of the extracellular and intracellular edges of ~30 Å wide membrane layer defined based on the biotin-avidin data for the PD. Dashed lines indicate 14 Å (top panel), 10 Å (middle panel), and 1 Å (bottom panel) vertical distance from the extracellular and intracellular edges of the membrane. Ca carbon atoms of the Kv1.2 residues corresponding to the KvAP residues studied by Ruta et al. (Ruta et al., 2005) (see sequence

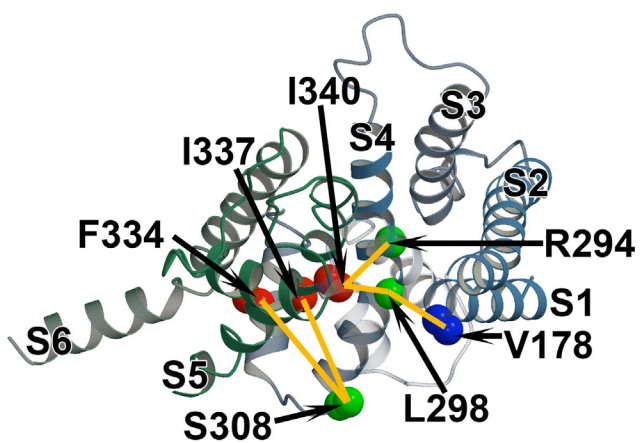
alignment in **Figure S5 in the Supplemental Data**) shown as spheres and colored as follows: red – residues which are accessible to avidin only from the extracellular side of the membrane; yellow – residues which are accessible to avidin from both sides of the membrane; black – residues which are inaccessible; blue - residues which are accessible to avidin only from the intracellular side of the membrane. Positions of selected residues discussed in the text indicated by arrow and labeled. The figure was generated using Molscript (Kraulis, 1991) and Raster3D (Merritt, 1997).

### KAT1 data mapped onto the Kv1.2 resting state model

**A**



**B**



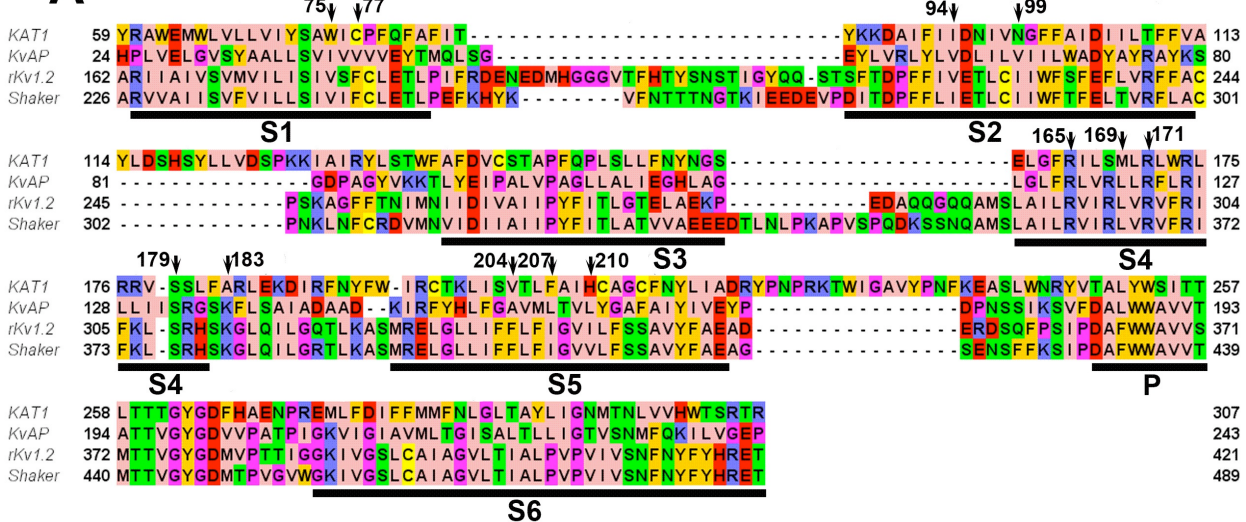
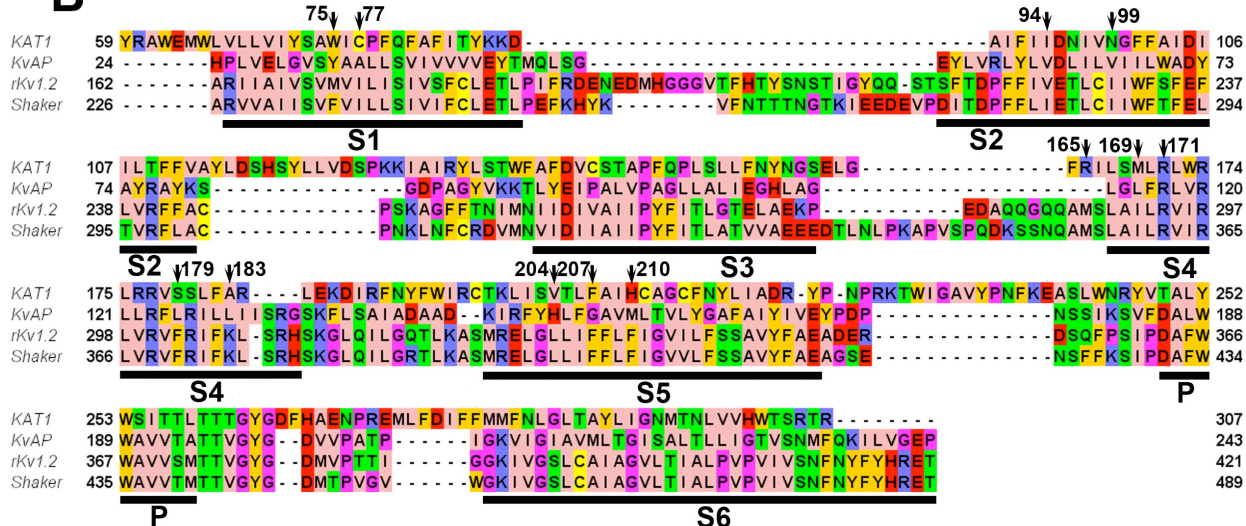
**Supplementary Figure S3. Interacting residues at the S4 and S5 interface in the down state of the KAT1 channel mapped onto the Kv1.2 resting state model**

(A) View of a single VSD from one subunit and PD from the adjacent subunit from the side of the membrane. Segments S1-S6 and S4-S5 linker are labeled accordingly. Ca and C $\beta$  carbon atoms of the Kv1.2 residues corresponding to the KAT1 residues identified by Grabe et al. (Grabe et al., 2007) (see sequence alignment in **Figure S4A in the Supplemental Data**) shown as spheres and colored red for S5 residues, green for S4 residues, and blue for

S1 residue. C $\beta$  carbon atoms of interacting residue pairs discussed in the text are connected by orange lines.

(B) View of the model shown in (A) from the extracellular side of the membrane. The figure was generated using Molscript (Kraulis, 1991) and Raster3D (Merritt, 1997).

Recently, Grabe et al. (Grabe et al., 2007) reported a number of experimentally derived constraints on the down state conformation of the VSD of the hyperpolarization-activated KAT1 channel. **Figure S3 in the Supplemental Data** shows residues proposed to be in close proximity between the S4 and S5 segments based on these data mapped onto the Kv1.2 resting state model using sequence alignment shown in **Figure S4A in the Supplemental Data**, which is significantly different from sequence alignment used by Grabe et al. (Grabe et al., 2007) (see **Figure S4B in the Supplemental Data**). Our resting state model shows that side chains of R294 and L298 in the middle of S4 of Kv1.2 (R165 and M169, respectively, in KAT1; R362 and L366 in Shaker) are positioned in very close proximity to the side chain of I340 in the middle of S5 (H210 in KAT1; V408 in Shaker), suggesting that the position of the middle region of S4 relative to the PD is similar in the down state of the VSD in both channels. Detailed analysis of the KAT1 data mapped onto the resting state model shows that the side chain of L298 in S4 (M169 in KAT1; L366 in Shaker) is positioned in close proximity to V178 in S1 (W75 in KAT1; V242 in Shaker), suggesting that the position of the middle region of S4 relative to the S1 is also similar in the down state of the VSD in both channels. Since the PD is open in the down state of the KAT1, it is likely that position of the S4-S5 linker and therefore of the C-terminal end of S4 maybe significantly different in the down state of the KAT1 from the resting state of the Kv1.2. Our resting state model shows that residue S308 at the C-terminal end of S4 (S179 in KAT1; S376 in Shaker) is at the same depth in the membrane as F334 and I337 at the N-terminal end of S5 (V204 and F207, respectively, in KAT1; and F402 and I405, respectively, in Shaker), however, the side chain of S308 in Kv1.2 points away from the S4 and S5 interface. Other KAT1 down state residue pairs identified by Grabe et al. (Grabe et al., 2007) are not within close proximity in our Kv1.2 resting state model (see **Figure S5 in the Supplemental Data**).

**A****B**

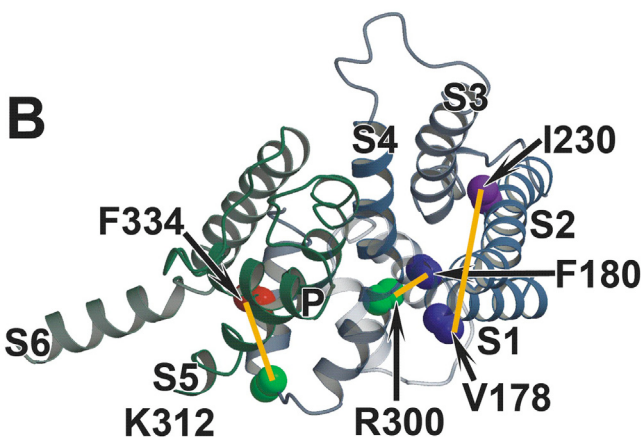
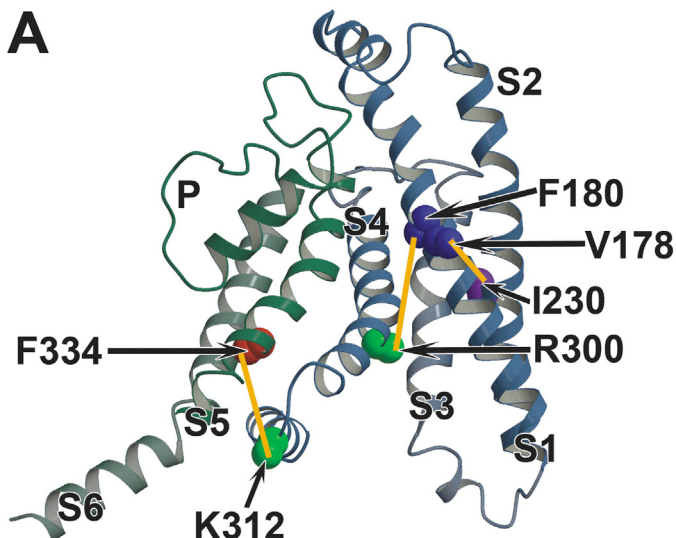
### Supplementary Figure S4.

(A) The amino acid sequence alignment of the transmembrane region of the KAT1, KvAP, rat Kv1.2, and Shaker Kv channel used to map interacting residues identified by Grabe et al.(Grabe et al., 2007) onto the Kv1.2 resting state model in **Figure 7** and **Supplementary Figure S5**. The alignment was generated using ClustalX software (Jeanmougin et al., 1998) and then manually adjusted based on the transmembrane regions in the KvAP VSD x-ray structure (Jiang et al., 2003) and Kv1.2 PD x-ray structure (Long et al., 2005a). Transmembrane segments from S1 through S6 and P helix in the selectivity filter underlined by black bars. Positions of interacting residues identified by Grabe et al. (Grabe et al., 2007) are labeled and marked by the arrow above the sequence alignment. Numbers on the left and right side of the alignment correspond to the first and last residue of that region of the sequence, respectively. Residues were colored with Jalview program (Clamp, 1999) using the Zappo color scheme, where hydrophobic residues (I, L, V, A, and M) are colored pink, aromatic residues (F, W, and Y) are colored orange, positively charged residues (K, R, and H)

are colored blue, negatively charged residues (D and E) are colored red, hydrophilic residues (S, T, N, and Q) are colored green, P and G colored magenta, and C is colored yellow.

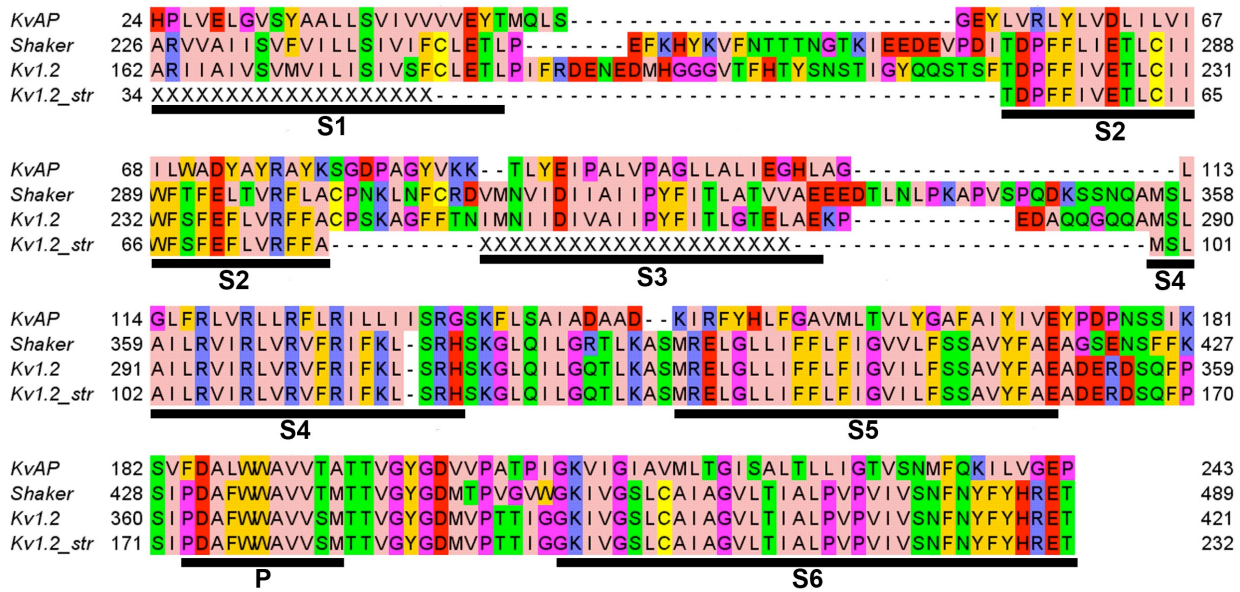
(B) The alignment used by Grabe et al. (Grabe et al., 2007) to model the down state of the KAT1 channel and the resting state of the Shaker Kv channel. The KvAP sequence was added based on alignment to Kv1.2 and Shaker Kv channel shown in **Supplementary Figure S6**. The alignment labeled and colored as in panel A.

We suggest that although packing of the middle of S4 and the middle of S5 may be similar in the down state of VSD in Kv1.2 and KAT1, packing of the intracellular parts of the VSD and PD may be different between these channels due to the different state of the PD.



**Supplementary Figure S5.** Interacting residues identified by Grabe et al. (Grabe et al., 2007) in the down state of the KAT1 channel mapped onto the Kv1.2 resting state model. Only a single VSD from one subunit and PD from the adjacent subunit are shown from the side of the membrane (left panel) and extracellular side of the membrane (right panel). Segments S1-S6 and S4-S5 linker are labeled accordingly.  $\text{Ca}$  and  $\text{C}\beta$  carbon atoms of the Kv1.2 residues corresponding to the KAT1 residues identified by Grabe et al. (Grabe et al., 2007) (see sequence alignment in **Supplementary Figure S4**) shown as spheres and colored red for S5

residues, green for S4 residues, and blue for S1 residue. C $\beta$  carbon atoms of interacting residue pairs discussed in the text are connected by orange lines. The figure was generated using Molscript (Kraulis, 1991) and Raster3D (Merritt and Bacon, 1997).



**Supplementary Figure S6.** The amino acid sequence alignment of the S1 through S6 segments of the KvAP, Shaker, Kv1.2, and Kv1.2 sequence from the x-ray structure (Long et al., 2005a). Unidentified residues in the Kv1.2 structure marked as “X” in the sequence of the S1 and S3 segments. Transmembrane segments from S1 through S6 and P helix in the selectivity filter underlined by black bars. The first and last unidentified residues in S1 correspond to A162 and F180 in the Kv1.2 sequence, respectively. The first and last unidentified residues in S3 correspond to I254 and L274 in the Kv1.2 sequence, respectively. Residues colored as described in **Supplementary Figure S4**. Numbers on the left and right side of the alignment correspond to the first and last residue of that region of the sequence.

## Supplemental Experimental Procedures

### Fluorescence measurements

**Molecular Biology and Oocyte preparation.** Site directed mutagenesis was done using the Quick Change Mutagenesis kit from Stratagene and confirmed by sequencing. Unless otherwise denoted the construct of the channel was Shaker H4  $\Delta$ 6-46/C245V/C462A as described previously (Gandhi et al., 2000). cRNA was transcribed using the T7 Ambion mMessage mMachine kit. Injection of the oocytes (50 nl mRNA, at 0.1-1 ng/nl), native cysteine blocking with tetraglycine maleimide, and attachment of the fluorophore tetramethylrhodamine-6-maleimide (TMRM) were as previously described (Pathak et al., 2005). One to 4 hours after injection oocytes were incubated for 20 minutes at room temperature with tetraglycine maleimide to block native cysteines. After injection oocytes were incubated for one or two days at 18°C before labeling. Labeling was done with 5-50  $\mu$ M TMRM in a high potassium solution (in mM: 92 KCl, 0.75 CaCl<sub>2</sub>, 1 MgCl<sub>2</sub>, 10 Hepes pH 7.5) or low potassium solution (in mM: 92 NaMes, 2 KCl, 0.75 CaCl<sub>2</sub>, 1 MgCl<sub>2</sub>, 10 Hepes pH 7.5) for 60 min on ice. Oocytes were kept in ND96 solution in the dark at 12°C until being voltage clamped at room temperature.

**Voltage Clamp Fluorometry and Analysis.** Two electrode voltage clamp fluorometry was performed as described previously (Mannuzzu et al., 1996), using a Dagan CA-1 amplifier (Dagan Corporation), illuminated with a 100W mercury arc lamp, on a Zeiss IM35 microscope, using a 20x 0.75 n.a. fluorescence objective (Nikon). Photometry was performed with a Hamamatsu HC120-05 photomultiplier tube. The voltage clamp, photomultiplier and Uniblitz shutter (Vincent Associates) were digitized and controlled by a Digidata-1200 board and PClamp 8 software (Axon Instruments). The bath solutions consisted of (in mM) 110 NaMES, 2 KMES, 2 CaMES<sub>2</sub>, 10 HEPES pH7.5 or 20 NaMES, 90 KMES, 2 CaMES<sub>2</sub>, 10 HEPES pH7.5. Oocytes were washed with the bath solution before being placed in the recording chamber. Light was filtered with a HQ TRITC filter cube (Chroma Technology). The voltage output of the photomultiplier was low-pass filtered with an 8-pole Bessel filter (Frequency Devices) and digitized at 10kHz. A minimum of a 2 min rest interval at the holding potential of -80 mV was given before steps to depolarizing voltages. Data analysis was done with the Axon Laboratory programs pClamp8 and Clampfit 9.2 (Axon Instruments) and

custom-prepared Matlab programs as described below. Fluorescence data for several sites from the PD and the S4 region was taken from Gandhi et al., (2000); please refer to Table 1 for the complete list.

## **Data Analysis**

**Formatting traces for analysis.** For each recording, fluorescence and current traces were imported as vectors in Matlab (Mathworks, Inc.) using script import\_abf.m available online from Matlab central file exchange. First the fluorescence trace was normalized so that the baseline fluorescence corresponded to 1. This allowed bleach correction by subtracting from the trace a normalized control fluorescence trace consisting of a recording without a voltage step. When a suitable control file was not present, bleach correction was done by subtracting from the trace the line that best fit the fluorescence decay that occurs prior and subsequent to the change in fluorescence associated with the voltage step.

**Evaluating parameters for sites.** The fluorescence response to the depolarizing step was fit by a double exponential. The two components of the fit correspond to channel activation and slow inactivation, as described in the **Results** section. Fit parameters for fluorescence traces from every cell were stored. From these, the amplitude of the fit to activation component (fast  $\Delta F$ ) was averaged across cells for a given site. Since the baseline fluorescence was normalized to 1, this value corresponds to the conventionally used representation,  $\Delta F/F$ .  $\Delta F$  values for all sites are expressed as percent changes and are reported in **Table 1**.

Color-coding for **Figure 3C** and **Figure S1B** was performed in the following manner: each site studied was attributed a color that represented its  $\Delta F$  magnitude. Values were normalized so that the largest  $\Delta F$  corresponded to the most saturated hue. Since the largest  $\Delta F$  could be orders of magnitude larger than the smallest,  $\Delta F$  values were transformed using the function  $f(x) = \tanh(c*x)$ , where  $c$  effectively corresponds to the degree of color amplification of sites with small  $\Delta F$ . For **Figure 3C**,  $c = 30$ .

## **Kv1.2 channel modeling**

**Modeling of the S6 in the resting state.** Experimental data suggests that the conformation of the S6 gate in the resting/closed state in the Shaker Kv channel differs from that observed in the x-ray structure of the KcsA channel (Doyle et al., 1998; Zhou et al., 2001). Cysteine residue substituted at position of V478 in Shaker (V410 in Kv1.2) remains accessible to a series of fairly large reagents in the resting state (del Camino et al., 2005; del Camino and Yellen, 2001). In particular, the mutant V478C provides a high affinity Cd<sup>2+</sup> binding site that can be reached in the resting state. This strongly suggests that the cysteine side chains at position of V478 are facing each other and located at the narrowest region of the helical bundle crossing in the closed state. These results are not compatible with the conformation of the S6 helices observed in the KcsA structure. Our model of the S6 conformation of the Kv1.2 channel was constructed to keep V410 accessible to the intracellular side of the membrane by treating the conserved PVP-motif in S6 as a hinge between two semi-rigid helical parts of S6. The concept of the PVP acting as a hinge is also supported by the Cd<sup>2+</sup> metal bridge between V476H and H486 stabilizing the open state of Shaker (Holmgren et al., 1998; Webster et al., 2004) and consistent with the distance between V408 and H418 observed in the Kv1.2 x-ray structure (Long et al., 2005a). The resting state model of the S6 of the Kv1.2 was obtained by energy minimization using CHARMM (Brooks et al., 1983). The S6 residues 404-421 were allowed to move during simulations. Residues 405-407 (PVP-motif) were allowed to alter their backbone conformation and the intracellular part of S6 (residues 408-421) moved as a semi-rigid body, the helical conformation being kept via a strong RMSD harmonic restraint. A harmonic restraining potential was used to impose a distance of ~5.5 Å between the Cβ atoms of V410 from adjacent subunits; this distance is typical of a Cd<sup>2+</sup> cysteine metal bridge.

**Homology/de novo modeling of the S4-S5 linker and S5 in the resting state.** The S4-S5 linker residues 311-324 (379-392 in Shaker) and the S6 residues 409-421 (477-489 in Shaker) were taken from the Kv1.2 open state structure (Long et al., 2005a) and superimposed over the S6 residues 409-421 onto our new model of the S6 in the resting state. Thus, in our new resting state model, the S4-S5 linker residues positioned exactly the same relative to the S6 residues as they are in the Kv1.2 open state structure (Long et al., 2005a). The same approach was used previously by Long et al. (Long et al., 2005b) to construct the resting state position of the S4-S5 linker of the Kv1.2 based on the KcsA

channel structure. The S5 residues 325-339 (393-407 in Shaker) were then modeled *de novo* within constrained positions of the S4-S5 linker and the remainder of the PD using the Rosetta-Membrane method (Yarov-Yarovoy et al., 2006b). 5,000 low-resolution models were generated and clustered as described previously (Bonneau et al., 2001). The center model of the largest cluster was chosen as the best model.

**Homology/de novo modeling of the Kv1.2 in open state.** Based on mapping of results of Miller group's tryptophan scan data for the S1 and S3 (Hong and Miller, 2000), Swartz group's alanine scan data for the S1-S4 (Li-Smerin et al., 2000), Papazian group's Mg<sup>2+</sup> binding data for residues in the S2 and S3 (Silverman et al., 2000), and Horn and Isacoff groups' MTS accessibility data for the S3 (Gandhi et al., 2003; Nguyen and Horn, 2002) onto the original Kv1.2 open state Rosetta-Membrane model (Yarov-Yarovoy et al., 2006a), we came to conclusion that sequence alignment between UNK residues in the S3 segment in the Kv1.2 open state structure (Long et al., 2005a) has to be moved by 3 positions from the original alignment (Yarov-Yarovoy et al., 2006a). In our new alignment, the first UNK residue in the S3 corresponds to I254 in the Kv1.2 sequence (V311 in Shaker) (see **Figure S6** in the Supplemental Data available). We rebuilt the Kv1.2 open state model using the original Rosetta-Membrane open state model (Yarov-Yarovoy et al., 2006a) as a template and modeled *de novo* the S1-S2, S2-S3, and S3-S4 loops. 5,000 low-resolution models were generated and clustered as described previously (Bonneau et al., 2001). The center model of the largest cluster was chosen as the best model (**Figure 7A**, left panel).

**Modeling of the VSD of Kv1.2 in the resting state.** The Rosetta-Membrane domain assembly method was used to model the VSD of Kv1.2 in the resting state. The Kv1.2 structure was divided into three regions: (i) the S1, S2, and the intracellular half of the S3 region (residues from A162 to I260); (ii) the *de novo* region for residues from V261 (I318 in Shaker; in the middle of S3) to G313 (G381 in Shaker; at the N-terminus of the S4-S5 linker); (iii) the S4-S5 linker and PD region (residues from L314 to T421 in Kv1.2; L382 to T489 in Shaker). The structural fragments library for the *de novo* region was generated as described previously (Rohl et al., 2004; Simons et al., 1999; Yarov-Yarovoy et al., 2006b). The x-ray structure of the Kv1.2 (Long et al., 2005a) was not used during the fragment library generation. The backbone coordinates of residues in the first and third regions were fixed in torsion but not Cartesian space and new structural fragment insertions were allowed only in

the second (*de novo*) region. The structure of the S1 and S2 and intracellular half of the S3 was taken from our new Kv1.2 open state model (see above). The structure of the S4-S5 linker and the PD was taken from the resting state PD model generated as described above. The starting structure for the extracellular half of S3 and the S3-S4 loop *de novo* region was our new Kv1.2 open state model. The starting structure for the S4 *de novo* region was manually adjusted based on the “steric” positions from the omega current scan data (Tombola et al., 2007) and constructed as follows - the S4 segment residues from M288 to L307 (M356 to L375 in Shaker) were excised from the Kv1.2 open state structure and superimposed onto the S4 position in the Kv1.2 open state structure so that the S4 region between R294 (R362 in Shaker; the first gating-charge-carrying arginine) and R300 (the third gating-charge-carrying arginine) was superimposed over the S4 region between R300 (R368 in Shaker) and K306 (K374 in Shaker). A single VSD was attached to a tetramer of the PD and starting conformation for each independent simulation had the VSD position relative to the PD the same as in our new Kv1.2 open state model (see **Figure 6A**, left panel). The PD position was fixed relative to the membrane bilayer based on the lowest membrane environment score (Yarov-Yarovoy et al., 2006b) for the PD along the membrane normal vector, which was defined from the tetrameric structure of the PD. The S1, S2, and the intracellular part of the S3 region was allowed to move freely around the PD and within membrane bilayer, however, to avoid sampling of non-native conformations of this region, the N- and C-terminal residues of the S1 and S2 were disfavored within the hydrophobic layer of the membrane during simulations.

The extracellular half of S3, S3-S4 loop and the S4 were chosen as the *de novo* region based on the fluorescence scan data suggesting that this region of the VSD goes through significant motion during gating. Recent experimental data suggested significant increase of the S4 tilt angle in the resting state (Ruta et al., 2005; Tombola et al., 2007). Position of the extracellular end of S4 was constrained to be near the extracellular end of S5 and S6 from the adjacent subunit to favor significant tilt of S4 and fit the omega-scan data (Tombola et al., 2007). In addition, experimental data by Tombola et al. (Tombola et al., 2005) suggesting proximity of the R1 in S4 (R294 in Kv1.2; R362 in Shaker) and E1 in S2 (E226 in Kv1.2; E283 in Shaker) were used to favor side chain proximity (centroid-centroid distance below 8 Å) during modeling. 5,000 low-resolution models were generated followed by clustering with RMSD threshold of 2.1 Å as described previously (Bonneau et al., 2001). Ten largest clusters of

models were visually inspected and only the fourth cluster (by size) had models with tilted S4. All 189 models from the fourth cluster were visually inspected based on the omega-scan data (Tombola et al., 2007), fluorescence scan data, and MTS reagents accessibility (Larsson et al., 1996) data. The center model of this cluster had the best fit to the available experimental data presented here and elsewhere (Larsson et al., 1996; Tombola et al., 2007; Tombola et al., 2005) and was subjected to an all-atom refinement protocol that relaxes all backbone and side-chain conformational degrees of freedom to minimize an all-atom potential of mean force for membrane proteins (Barth et al., 2007). This full-atom potential is an extension of the Rosetta full-atom potential developed previously for water-soluble protein structure prediction and design calculations (Kuhlman and Baker, 2000), and describes interactions between membrane protein residues at atomic details while the water, hydrophobic core and lipid headgroup regions of the membrane are treated using continuum models. This full-atom potential consists of a linear combination of a Lennard-Jones potential that models Van der Waals attractive and repulsive atomic forces, a backbone torsional term that accounts for the different local structural propensities of the amino-acids, a knowledge-based pair interaction term that approximates electrostatic interactions between protein side-chains, 20 reference energies that control the overall amino-acid composition, an implicit atomic solvation term based on the model developed by Lazaridis and Karplus (Lazaridis and Karplus, 1999) and an orientation-dependent hydrogen bonding term (Kortemme et al., 2003). Both the solvation and the hydrogen-bond potentials were modified to account for the anisotropic membrane environment. In our model, solvation effects in the membrane bilayer are treated implicitly with a continuum solvent model. The modeling of the membrane is conceptually close to that developed by Lazaridis (Lazaridis, 2003) in his extension of EFF1 for membrane lipid bilayers, IMM1. The membrane environment is described using three continuum phases: two isotropic phases (polar headgroup / water and the hydrophobic core of the lipid bilayer) and one anisotropic phase in between (hydrophobic / polar headgroup interface region of the membrane). An implicit atomic solvation potential was derived for the hydrophobic phase based largely on experimental transfer free energies of peptides from water to non-polar solvents. The atomic solvation energies in the water phase are identical to those used in the energy function for water-soluble proteins. The atomic solvation energies in the membrane interface region are derived by interpolating the solvation properties from the two adjacent phases based on the depth of each atom in the membrane. Protein/lipid interactions are treated implicitly through the solvation energies and the effect of solvent-exposure on the

strength of hydrogen-bonds between protein atoms. 200 all-atom relaxed models were generated for each selected coarse-grained model and the lowest energy model that satisfied the experimental data (see above) was selected as the best model.

**$\Delta$ SASA calculations.** Change in residue solvent-accessible surface area ( $\Delta$ SASA) was calculated between the Kv1.2 resting and open state models (see Results and Discussion) for each VSD position studied using the WHATIF server (<http://swift.cmbi.kun.nl/WIWWWI/access3.html>) and then normalized to a ratio of TMRM probe volume to residue side chain volume at each position to reflect  $\Delta$ SASA of TMRM probe.

**Gating Charge Calculation.** Kv1.2 models were refined by energy minimization using the program CHARMM (Brooks et al., 1983). The gating charge was calculated from the structural models of the open and closed states using the modified Poisson–Boltzmann voltage equation (Roux, 1997) implemented in the finite-difference PBEQ module of CHARMM. The method used is the same as described in Chanda et al (Nature, 2005). A dielectric of 2 was assigned to the protein, and the protein–solvent interface was determined using the set of optimized atomic Born radii (Nina et al., 1997). The membrane was represented as a 24 Å slab of low dielectric 2, assembled by packing lipid hydrocarbon chains (explicitly represented) around the channel; all aqueous crevices of the pore and voltage sensor were represented as high dielectric regions of 80. A grid of 160 point with a spacing of 1 Å was used.

## Supplementary Table I.

Vertical Movement of Residues in the S4 Segment of the Kv1.2 channel between the Resting/Closed and Activated/Open States.

<i>Kv1.2 Residue Number</i>	$D_c$ , Å
M288	9.6
S289	14.3
L290	11.4
A291	6.8
I292	10.8
L293	13.2
<b>R294</b>	<b>8.0</b>
V295	7.1
I296	11.7
<b>R297</b>	<b>10.5</b>
L298	5.0
V299	5.6
<b>R300</b>	<b>10.4</b>
V301	7.2
F302	3.5
<b>R303</b>	<b>7.4</b>
I304	6.5
F305	1.1
K306	1.9
L307	4.1
S308	-0.7
R309	-3.9
H310	-1.5
<b>Average</b>	<b>6.5±4.8</b>

Change of vertical position of C $\alpha$  atoms of residues in the S4 of the Kv1.2 between the resting (closed) and activated (open) states ( $\Delta D_{C\alpha}$ ) measured along the membrane normal and relative to C $\alpha$  atom position of GYG residues in the selectivity filter (G376, Y377, and G378 in the Kv1.2). Residues shown in bold are the gating charge-carrying arginines in the S4. The bottom row of the table shows the average and standard deviation values over all residues of the S4.

## Supplemental References

- Armstrong, C. M., and Loboda, A. (2001). A model for 4-aminopyridine action on K channels: similarities to tetraethylammonium ion action. *Biophys J* 81, 895-904.
- Barth, P., Schonbrun, J., and Baker, D. (2007). Efficient all-atom modeling of interactions, structural specificities and helical distortions in membrane proteins. *Proc Natl Acad Sci U S A*, in press.
- Bonneau, R., Strauss, C. E., and Baker, D. (2001). Improving the performance of Rosetta using multiple sequence alignment information and global measures of hydrophobic core formation. *Proteins* 43, 1-11.
- Brooks, B. R., Brucolieri, R. E., Olafson, B. D., States, D. J., Swaminathan, S., and Karplus, M. (1983). CHARMM: A Program for Macromolecular Energy Minimization and Dynamics Calculations. *J Comp Chem* 4, 187-217.
- Clamp, M. E., Cuff, J. A. and Barton, G. J. (1999). Jalview- a java multiple sequence alignment viewer and editor. <http://wwwebiacuk/~michele/jalview>.
- del Camino, D., Kanevsky, M., and Yellen, G. (2005). Status of the intracellular gate in the activated-not-open state of shaker K<sup>+</sup> channels. *J Gen Physiol* 126, 419-428.
- del Camino, D., and Yellen, G. (2001). Tight steric closure at the intracellular activation gate of a voltage-gated K(+) channel. *Neuron* 32, 649-656.
- Doyle, D. A., Morais Cabral, J., Pfuetzner, R. A., Kuo, A., Gulbis, J. M., Cohen, S. L., Chait, B. T., and MacKinnon, R. (1998). The structure of the potassium channel: molecular basis of K<sup>+</sup> conduction and selectivity. *Science* 280, 69-77.
- Gandhi, C. S., Clark, E., Loots, E., Pralle, A., and Isacoff, E. Y. (2003). The orientation and molecular movement of a K(+) channel voltage-sensing domain. *Neuron* 40, 515-525.
- Gandhi, C. S., Loots, E., and Isacoff, E. Y. (2000). Reconstructing voltage sensor-pore interaction from a fluorescence scan of a voltage-gated K<sup>+</sup> channel. *Neuron* 27, 585-595.
- Grabe, M., Lai, H. C., Jain, M., Nung Jan, Y., and Yeh Jan, L. (2007). Structure prediction for the down state of a potassium channel voltage sensor. *Nature* 445, 550-553.
- Holmgren, M., Shin, K. S., and Yellen, G. (1998). The activation gate of a voltage-gated K<sup>+</sup> channel can be trapped in the open state by an intersubunit metal bridge. *Neuron* 21, 617-621.
- Hong, K. H., and Miller, C. (2000). The lipid-protein interface of a Shaker K(+) channel. *J Gen Physiol* 115, 51-58.
- Jeanmougin, F., Thompson, J. D., Gouy, M., Higgins, D. G., and Gibson, T. J. (1998). Multiple sequence alignment with Clustal X. *Trends Biochem Sci* 23, 403-405.
- Jiang, Y., Lee, A., Chen, J., Ruta, V., Cadene, M., Chait, B. T., and MacKinnon, R. (2003). X-ray structure of a voltage-dependent K<sup>+</sup> channel. *Nature* 423, 33-41.
- Kortemme, T., Morozov, A. V., and Baker, D. (2003). An orientation-dependent hydrogen bonding potential improves prediction of specificity and structure for proteins and protein-protein complexes. *J Mol Biol* 326, 1239-1259.
- Kraulis, P. J. (1991). MOLSCRIPT: a program to produce both detailed and schematic plots of protein structures. *J Appl Crystallogr* 24, 946-950.
- Kuhlman, B., and Baker, D. (2000). Native protein sequences are close to optimal for their structures. *Proc Natl Acad Sci U S A* 97, 10383-10388.
- Larsson, H. P., Baker, O. S., Dhillon, D. S., and Isacoff, E. Y. (1996). Transmembrane movement of the shaker K<sup>+</sup> channel S4. *Neuron* 16, 387-397.
- Lazaridis, T. (2003). Effective energy function for proteins in lipid membranes. *Proteins* 52, 176-192.
- Lazaridis, T., and Karplus, M. (1999). Effective energy function for proteins in solution. *Proteins* 35, 133-152.
- Ledwell, J. L., and Aldrich, R. W. (1999). Mutations in the S4 region isolate the final voltage-dependent cooperative step in potassium channel activation. *J Gen Physiol* 113, 389-414.
- Li-Smerin, Y., Hackos, D. H., and Swartz, K. J. (2000). alpha-helical structural elements within the voltage-sensing domains of a K(+) channel. *J Gen Physiol* 115, 33-50.
- Long, S. B., Campbell, E. B., and Mackinnon, R. (2005a). Crystal structure of a mammalian voltage-dependent Shaker family K<sup>+</sup> channel. *Science* 309, 897-903.

- Long, S. B., Campbell, E. B., and MacKinnon, R. (2005b). Voltage sensor of Kv1.2: structural basis of electromechanical coupling. *Science* *309*, 903-908.
- Loots, E., and Isacoff, E. Y. (1998). Protein rearrangements underlying slow inactivation of the Shaker K<sup>+</sup> channel. *J Gen Physiol* *112*, 377-389.
- McCormack, K., Joiner, W. J., and Heinemann, S. H. (1994). A characterization of the activating structural rearrangements in voltage-dependent Shaker K<sup>+</sup> channels. *Neuron* *12*, 301-315.
- Merritt, E. A., and Bacon, D.J. (1997). Raster3D: Photorealistic Molecular Graphics. *Methods Enzymol* *277*, 505-524.
- Nguyen, T. P., and Horn, R. (2002). Movement and crevices around a sodium channel S3 segment. *J Gen Physiol* *120*, 419-436.
- Nina, M., Belgov, D., and Roux, B. (1997). Atomic Born radii for continuum electrostatic calculations based on molecular dynamics free energy simulations. *J Phys Chem B* *101*, 5239-5248.
- Pathak, M., Kurtz, L., Tombola, F., and Isacoff, E. (2005). The cooperative voltage sensor motion that gates a potassium channel. *J Gen Physiol* *125*, 57-69.
- Perozo, E., MacKinnon, R., Bezanilla, F., and Stefani, E. (1993). Gating currents from a nonconducting mutant reveal open-closed conformations in Shaker K<sup>+</sup> channels. *Neuron* *11*, 353-358.
- Rohl, C. A., Strauss, C. E., Misura, K. M., and Baker, D. (2004). Protein structure prediction using Rosetta. *Methods Enzymol* *383*, 66-93.
- Roux, B. (1997). Influence of the membrane potential on the free energy of an intrinsic protein. *Biophys J* *73*, 2980-2989.
- Ruta, V., Chen, J., and MacKinnon, R. (2005). Calibrated measurement of gating-charge arginine displacement in the KvAP voltage-dependent K<sup>+</sup> channel. *Cell* *123*, 463-475.
- Silverman, W. R., Tang, C. Y., Mock, A. F., Huh, K. B., and Papazian, D. M. (2000). Mg(2+) modulates voltage-dependent activation in ether-a-go-go potassium channels by binding between transmembrane segments S2 and S3. *J Gen Physiol* *116*, 663-678.
- Simons, K. T., Ruczinski, I., Kooperberg, C., Fox, B. A., Bystroff, C., and Baker, D. (1999). Improved recognition of native-like protein structures using a combination of sequence-dependent and sequence-independent features of proteins. *Proteins* *34*, 82-95.
- Tombola, F., Pathak, M. M., Gorostiza, P., and Isacoff, E. Y. (2007). The twisted ion-permeation pathway of a resting voltage-sensing domain. *Nature* *445*, 546-549.
- Tombola, F., Pathak, M. M., and Isacoff, E. Y. (2005). Voltage-sensing arginines in a potassium channel permeate and occlude cation-selective pores. *Neuron* *45*, 379-388.
- Webster, S. M., Del Camino, D., Dekker, J. P., and Yellen, G. (2004). Intracellular gate opening in Shaker K<sup>+</sup> channels defined by high-affinity metal bridges. *Nature* *428*, 864-868.
- Yang, Y., Yan, Y., and Sigworth, F. J. (1997). How does the W434F mutation block current in Shaker potassium channels? *J Gen Physiol* *109*, 779-789.
- Yarov-Yarovoy, V., Baker, D., and Catterall, W. A. (2006a). Voltage sensor conformations in the open and closed states in ROSETTA structural models of K(+) channels. *Proc Natl Acad Sci U S A* *103*, 7292-7297.
- Yarov-Yarovoy, V., Schonbrun, J., and Baker, D. (2006b). Multipass membrane protein structure prediction using Rosetta. *Proteins* *62*, 1010-1025.
- Zhou, Y., Morais-Cabral, J. H., Kaufman, A., and MacKinnon, R. (2001). Chemistry of ion coordination and hydration revealed by a K<sup>+</sup> channel-Fab complex at 2.0 Å resolution. *Nature* *414*, 43-48.